

Structural relations between two ground states of NaV_2O_5 under high pressure: A synchrotron x-ray diffraction study

Kenji Ohwada,^{1,*} Yasuhiko Fujii,² Jiro Muraoka,^{3,†} Hironori Nakao,⁴ Youichi Murakami,⁴ Yukio Noda,⁵ Hiroyuki Ohsumi,⁶ Naoshi Ikeda,^{6,‡} Takahisa Shobu,¹ Masahiko Isobe,⁷ and Yutaka Ueda⁷

¹Quantum Beam Science Directorate (in SPring-8), Japan Atomic Energy Agency, 1-1-1 Kouto, Sayo, Sayo-gun, Hyogo 679-5148, Japan

²Quantum Beam Science Directorate, Japan Atomic Energy Agency, 2-4 Shirane, Shirakata, Tokai, Ibaraki 319-1195, Japan

³Neutron Science Laboratory, Institute for Solid State Physics, The University of Tokyo, 106-1, Shirakata, Tokai, Ibaraki 319-1106, Japan

⁴Department of Physics, Tohoku University, Sendai, Miyagi 980-8578, Japan

⁵Institute of Multidisciplinary Research for Advanced Materials, Tohoku University, Sendai, Miyagi 980-8577, Japan

⁶Japan Synchrotron Radiation Research Institute (SPring-8), 1-1-1 Kouto, Sayo, Sayo-gun, Hyogo 679-5198, Japan

⁷Materials Design and Characterization Laboratories, Institute for Solid State Physics, The University of Tokyo, 5-1-5 Kashiwanoha, Kashiwa, Chiba 277-8581, Japan

(Received 5 July 2007; published 26 September 2007)

Structural relations between two ground states of the axial next nearest neighbor Ising compound NaV_2O_5 , $C_{1/4}$ and C_0 phases below and above the transition pressure $P_C=1$ GPa, were investigated by x-ray diffraction and scattering techniques. The structure of the C_0 phase is well explained by the A (A') pattern, which is one of four layers ($AAA'A'$) of the $C_{1/4}$ phase, however, the amount of the atomic shifts under the conditions 1.6 GPa and 6 K is 27% that under ambient pressure. On the other hand, resonant x-ray scattering showed that the charges are disproportionated under high pressure. Based on these facts, it was concluded that charge disproportionation corresponds to the Ising variable in NaV_2O_5 , where the atomic shifts are regarded as linearly coupled to the Ising spins. These results lead to the hypothesis that the competitive interactions between the Ising spins may result from the Ising spin-phonon coupling.

DOI: 10.1103/PhysRevB.76.094113

PACS number(s): 71.27.+a, 61.10.Nz, 62.50.+p

I. INTRODUCTION

The most exciting phase diagram in statistical physics—the *devil's flower*—has been reproduced perfectly in a temperature-pressure (T - P) phase diagram of NaV_2O_5 as shown in Fig. 1.^{1,2} Application of high pressure changes the lattice modulation along the c axis of NaV_2O_5 drastically. Precise x-ray diffraction experiment makes it clear that a large number of transitions successively take place among higher-order commensurate phases with $2a \times 2b \times zc$ type superstructures,^{1,2} where $a \times b \times c$ is the orthorhombic unit cell under ambient conditions. The arrangement of the modulation wave number along the c axis q_c , defined by $1/z$ and attached to “C” in Fig. 1(a), corresponds perfectly to that in the devil's flower in Fig. 1(b).

The devil's flower [see Fig. 1(b)] was first modeled by Bak and von Boehm in 1980. They proposed the simple model which is now well known as axial next nearest neighbor Ising (ANNNI) model.^{3,4} On the basis of the model, they carried out theoretical calculations in consideration of two competitive interlayer interactions between Ising spins [see Fig. 1(b) inset], i.e., the nearest neighbor interaction $J_1 \geq 0$ (ferro) and the next nearest neighbor interaction $J_2 \leq 0$ (antiferro), and finally obtained an interesting κ - T ($\kappa = -J_2/J_1$) phase diagram [see Fig. 1(b)], in which an infinite number of commensurate phases appear as a function of κ and T . Such a complicated phase diagram is named devil's flower because it seems as if an infinite number of petals bloom from the $\kappa=1/2$ position. It is essentially important that there are only two stable ground states as $T \rightarrow 0$, i.e., $\uparrow\uparrow\uparrow\dots$ (ferro, all

up configuration, $q=0$) state for $-J_2/J_1 \geq 1/2$ and $\uparrow\uparrow\downarrow\downarrow\uparrow\uparrow\downarrow\downarrow\dots$ (up-up-down-down configuration, $q=1/4$) state for $-J_2/J_1 \leq 1/2$.

In NaV_2O_5 ,⁵ which is well described as a quarter-filled two-leg ladder system,⁶⁻⁸ all vanadium ions have an average oxidation state of +4.5 ($\text{V}^{4.5+}$) at room temperature: one electron is distributed on one V—O—V rung. At $T_C=34$ K, NaV_2O_5 undergoes a novel cooperative phase transition associated with its charge disproportionation ($2\text{V}^{4.5+} \rightarrow \text{V}^{4+} + \text{V}^{5+}$),⁹ lattice dimerization ($2a \times 2b \times 4c$ superstructure),¹⁰ and spin-gap formation ($\Delta=9.8$ meV).^{10,11} The complementary use of x-ray structural analysis and the resonant x-ray scattering (RXS) techniques¹²⁻¹⁵ led us to the unique solution of the superstructure at ambient pressure. It was determined that the structure of $C_{1/4}$ phase at ambient pressure is crystallographically $(a-b) \times 2b \times 4c$ with the space group $C_2^2 - A112$ (No. 5, monoclinic) (see Fig. 2).^{16,17} An oblique charge stripe pattern formed in each V_2O_5 layer (ab plane) is shown in Fig. 2 as A (A') and its domains B (B'), respectively, where a black pyramid represents V^{4+}O_5 and a white pyramid represents V^{5+}O_5 . Atomic shifts coupled with the charge ordering are not shown in this figure. The charge ordering patterns called A (B) and A' (B') are related by a phase shift by π along the b axis. The stacking sequence of the charge-ordered ab plane (A , A' , B , and B') along the c axis was unequivocally determined by RXS as $AAA'A'$ ($BBB'B'$) by focusing on monoclinic single domain.¹³⁻¹⁵

In this way, a series of detailed structural studies gave us a possible characterization of the true character of the Ising variable in NaV_2O_5 . Since the temperature-pressure phase

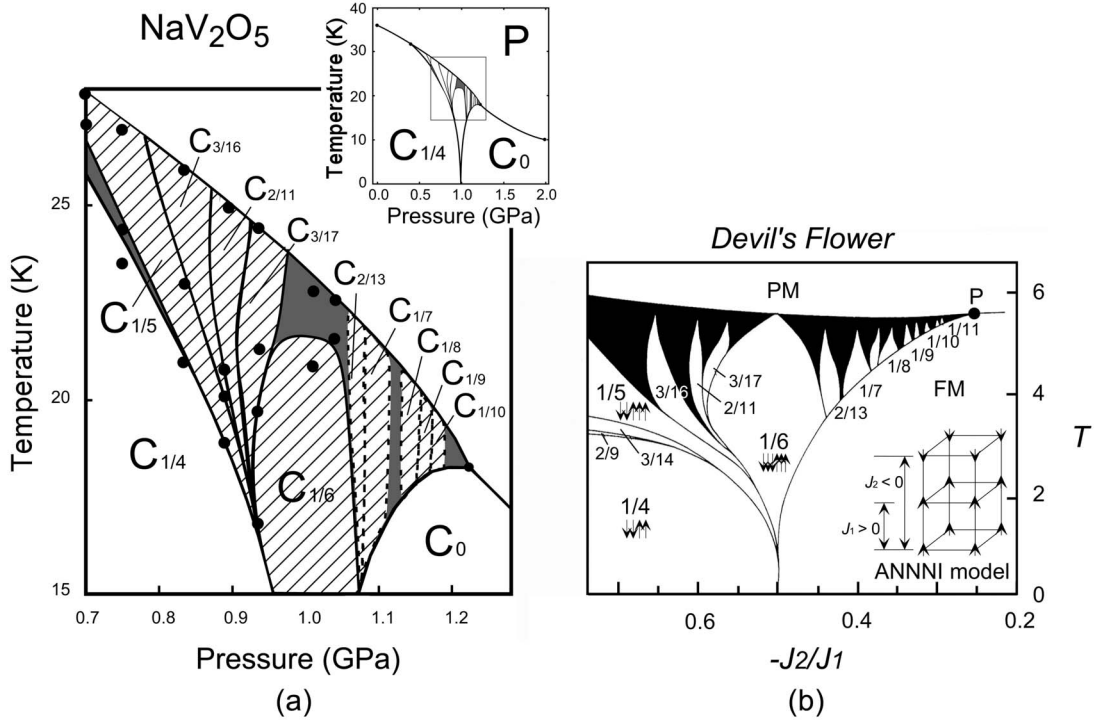


FIG. 1. (a) T - P phase diagram “devils flower” of NaV₂O₅ (Ref. 1). The hatched area shows commensurate phases unequivocally identified, while the shaded area indicates more complicated higher-order commensurate or incommensurate phases. (b) Devil’s flower (κ - T phase diagram) obtained from ANNNI model (Refs. 3 and 4). Fractions seen in the phase diagram show the modulation wave numbers. Black regions are composed of more complicated commensurate and incommensurate phases.

diagram previously observed in NaV₂O₅ (Refs. 1 and 2) very closely resembles the κ - T global phase diagram of the ANNNI model, it is quite reasonable to understand that the low-temperature structure of $C_{1/4}$ phase with the AAA'A' sequence corresponds to the phase of $q=1/4$ with an $\uparrow\uparrow\downarrow\downarrow$ configuration of the ANNNI model. That is to say, Ising spins \uparrow and \downarrow are equivalent to the charge order patterns A and A'.¹⁵

In order to secure positive evidence supporting this conjecture, in the present study, we particularly focused on the relationship between the two ground states of NaV₂O₅ below and above $P_C=1$ GPa.² The ground state below P_C ($C_{1/4}$ phase) is now well known, but the ground state above P_C (C_0 phase) is not yet understood. If the structure of the C_0 phase is explained by the A pattern, this will prove that the above conjecture is correct. That is to say, if the ground state under high pressure can be simply explained by the A pattern, we can conclude that the A and A' patterns make up all the Cq_c phases, for example, AAA'A'A'... ($C_{1/5}$ phase), AAAA'A'A'... ($C_{1/6}$ phase), AAAA'A'AAAA'A'A'... ($C_{2/11}$ phase), and so on.

The present paper is organized as follows: The experimental details are given in Sec. II. In Sec. III, we show the result of model calculation for the structural determination of the C_0 phase. We will demonstrate that the structure of the C_0 phase can be explained as consisting of one layer (A or A') extracted from the $C_{1/4}$ phase on condition that the amount of atomic shifts decreases under high pressure. In Sec. IV, we will also show the result of our RXS study. The present RXS study revealed the charge disproportionation

which occurs in spite of the decrement of the atomic shifts. Discussion is presented in Sec. V. In Sec. V, we will discuss Ising spin-phonon coupling, which may be a nature of the competitive interaction J_1 and J_2 along the c axis. It is already understood that an intersite Coulomb interaction between d^1 electrons on the V sites is essential for the charge disproportionation in the ab plane,⁷ but the origin of the competitive interaction (J_1 and J_2) which generates the long periodic superstructure has not yet been found.

II. EXPERIMENT

A. Collection of intensity data under low temperature and high pressure

In order to determine the structure of the C_0 phase, we performed an x-ray diffraction experiment under low temperature and high pressure (LTHP) on a four circle diffractometer installed at BL02B1 (SPring-8). Intensity vs $Q(hkl)$ data at 6 K and 1.6 GPa were carefully collected by the ω -scan method using a scintillation counter. Wavelength was tuned to 0.4292 Å (28.89 keV) with a Si(111) double-crystal monochromator. For the LTHP experiments, a conventional He-gas-driven diamond anvil cell (DAC) was mounted on a closed-cycle He-gas refrigerator. Pressure was generated in the DAC using a 1:1 mixture of *n*-pentane:*i*-pentane pressure transmitting media and was calibrated from a lattice constant of NaCl single crystal¹⁸ enclosed with the specimen in the DAC. The sample temperature was monitored with a Si-diode sensor directly attached to the DAC. We used as-

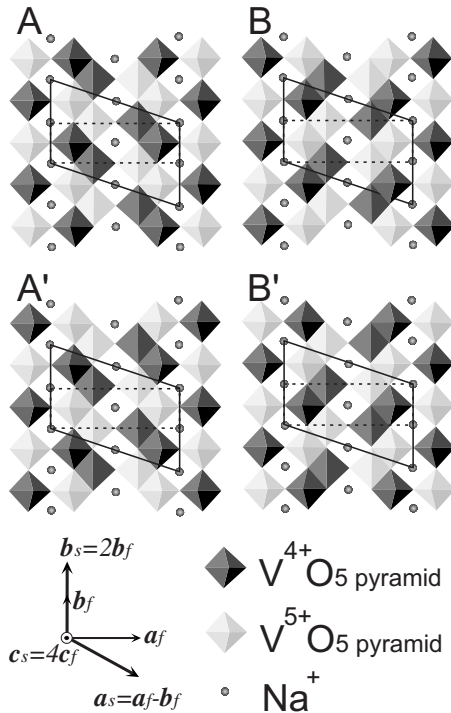


FIG. 2. Charge order patterns determined in ab plane, consisting of two kinds of patterns A and A' , and their domains B and B' . A and its domain B patterns coexist inevitably on the same layer because of the loss of a mirror symmetry perpendicular to the a or b axis (m_x, m_y) by the phase transition (twin rule). Dotted and solid lines represent the unit cells above and below T_C , respectively. The vectors represent the direction and length of each axis, where f denotes fundamental and s denotes superlattice. The black pyramid represents $V^{4+}O_5$ and white pyramid represents $V^{5+}O_5$ (Refs. 16 and 17).

grown high quality and small single crystal of NaV_2O_5 with a typical size of $75 \times 150 \times 20 \mu m^3$ ($a \times b \times c$) grown by the same method as previously reported.^{5,19} Finally, we could access 18 fundamental Bragg points and 53 superlattice Bragg points. No peak splitting originating from monoclinic symmetry was observed at 1.6 GPa and 6 K. We confirmed that the amount of split angle decreases as the pressure increases. However, this is not a pattern contradictory to the domain structure.

We mention here that the hydrostatic condition is realized at room temperature at 1 GPa, while nonhydrostatic condition under low temperature at 1 GPa. The pressure distribution inside the DAC chamber is estimated as $\Delta P \sim 0.1$ GPa.¹ We have controlled the pressure change within 0.1 GPa from room temperature (RT) to ~ 6 K, and no nonhydrostatic-pressure effect has been observed. We also add that the samples are from the same growth batch at a series of the experiments.

B. Resonant x-ray scattering study under low temperature and high pressure

Since the 5.47 keV (energy of the K -absorption edge of vanadium) x-ray cannot penetrate the diamond anvils, we

have, thus, developed a He-gas-driven DAC for RXS (RXS-DAC).²⁰ As shown in Fig. 3(a), 5.47 keV x rays come into and out of the sample chamber through the Be gasket. For the LTHP experiments, RXS-DAC was mounted on a closed-cycle He-gas refrigerator. Experiments were performed on a four circle diffractometer installed at BL-16A2 (Photon Factory). Sampling, pressure determination, and other operations were carried out in the same way as in the previous experiment shown in Sec. II A. A typical size of samples was $150 \times 350 \times 50 \mu m^3$ ($a \times b \times c$). We kept the $\epsilon_i \parallel c$ configuration all the time, where ϵ_i is the electric field vector of incident x ray. Because the K -edge spectra from NaV_2O_5 exhibit linear dichroism,^{21–23} the intensity at pre-edge has a large azimuthal angle dependence (strongest when $\epsilon_i \parallel c$), while there is no dependence at the main edge. The difference in the azimuthal angle dependence is caused by a transition mechanism of core electron.²⁴

C. Fluorescence measurements under high pressure

Fluorescence spectra under high pressure (HP) at RT were independently taken at the XAFS station of BL22XU (SPring-8).²⁵ A 19-element solid state detector (19-SSD) was employed for precise measurements of fluorescence from a small crystal of NaV_2O_5 in a DAC. As seen in Fig. 3(b), the 19-SSD was set at 90° direction in a horizontal plane, where the polarization of the incident x ray is π_i . For a large $c \parallel \epsilon_i$ component and for a large acceptance angle at the ab plane, the sample was inclined by about 30° from $k_i \parallel b$ as shown in Fig. 3(b). The size of the crystal in the RXS-DAC was $100 \times 50 \times 50 \mu m^3$ ($a \times b \times c$).

III. STRUCTURE DETERMINATION OF THE C_0 PHASE

Since the amount of collectable diffraction data from a sample in the DAC is limited and they are less than the number of structure parameters used for the present analysis, we define a convergence policy: the present analysis will be successful when the layer extracted from the $C_{1/4}$ phase can describe the C_0 phase with three adjustable parameters, α for the amount of the atomic shift, β for the thermal parameter, and γ for the domain ratio. The details of the parameters will be explained next.

As mentioned in Sec. I, the characteristic sequence of the $C_{1/4}$ phase is $AAA'A'$. The space group is $A112$ with an $(a-b) \times 2b \times 4c$ unit cell.^{16,17} Here, A and A' patterns are connected by an A lattice and 2_1 screw axis in the $A112$ space group. Meanwhile, we hypothesize that the pattern in C_0 phase is $AAAA$ with an $(a-b) \times 2b \times c$ unit cell. This pattern is easily introduced by eliminating the A lattice and 2_1 screw axis from the $A112$ space group. That is, the space group is $P112$ with an $(a-b) \times 2b \times c$ unit cell. The unit cell size and symmetry operation in this space group are shown in Fig. 4.

We used one layer from the $C_{1/4}$ phase ($AAA'A'$ sequence) determined by Ninomiya¹⁷ at ambient pressure, the A pattern as shown in Fig. 4. The A pattern satisfies the requirements of the estimated space group $P112$, where there are four independent Na sites, four independent V sites, and ten independent O sites. All independent atoms are labeled as

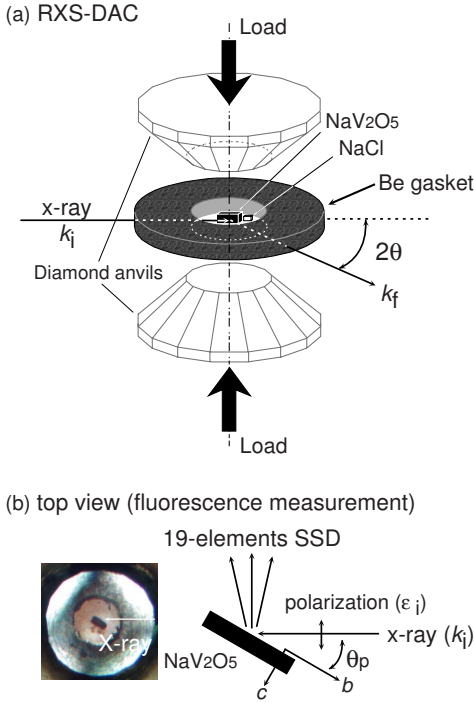


FIG. 3. (Color online) (a) The layout of RXS-DAC. 5.47 keV x ray comes into and out of the sample chamber through the Be gasket. Four windows opened on DAC jacket, each with 70° equatorial, allow the collection of high-angle diffraction of NaV_2O_5 through the Be gaskets. Our target reflection $(7.5, 0.5, L)$ locates at $2\theta \sim 100^\circ$ when the incident x-ray energy is 5.47 keV. (b) Geometry (top view) of the fluorescence measurement under high pressure. 19-SSD was set at the 90° direction in a horizontal plane, where the polarizations of the incident x ray is π_i . Sample was set to give the $c \parallel \epsilon_i$ component and got the acceptance by the ac plane, where the sample was inclined by about 30° ($=\theta_p$) from $k_i \parallel b$.

seen in Fig. 4. Next, we derived the atomic coordinates $(x, y, z)_{10 \text{ K}}^{0.1 \text{ MPa}}$ and temperature factor $\mathbf{B}_{10 \text{ K}}^{0.1 \text{ MPa}}$ of the A pattern from Ref. 17, where z is quadrupled to adapt to the condition $q_c=0$. For easy calculation with the model of the C_0 phase, we separate the atomic coordinates $(x, y, z)_{10 \text{ K}}^{0.1 \text{ MPa}}$ into two parts as follows:

$$(x, y, z)_{10 \text{ K}}^{0.1 \text{ MPa}} = (x, y, z)_{100 \text{ K}}^{0.1 \text{ MPa}} + (\Delta x, \Delta y, \Delta z)_{10 \text{ K}}^{0.1 \text{ MPa}}, \quad (1)$$

where $(x, y, z)_{100 \text{ K}}^{0.1 \text{ MPa}}$ is the atomic coordinate at 100 K (above T_C , $Pm\bar{m}n$) adapted to the $P112$ setting and $(\Delta x, \Delta y, \Delta z)_{10 \text{ K}}^{0.1 \text{ MPa}}$ is the atomic shift of each atom at 10 K. They are listed in Table I. Finally, we define the atomic coordinates $(x, y, z)_{6 \text{ K}}^{1.6 \text{ GPa}}$ and temperature factor $\mathbf{B}_{6 \text{ K}}^{1.6 \text{ GPa}}$ of the C_0 phase as follows:

$$(x, y, z)_{6 \text{ K}}^{1.6 \text{ GPa}} = (x, y, z)_{100 \text{ K}}^{0.1 \text{ MPa}} + \alpha(\Delta x, \Delta y, \Delta z)_{10 \text{ K}}^{0.1 \text{ MPa}}, \quad (2)$$

$$\mathbf{B}_{6 \text{ K}}^{1.6 \text{ GPa}} = \beta^2 \mathbf{B}_{10 \text{ K}}^{0.1 \text{ MPa}}, \quad (3)$$

where α and β are the adjustable parameters for the present model calculation.

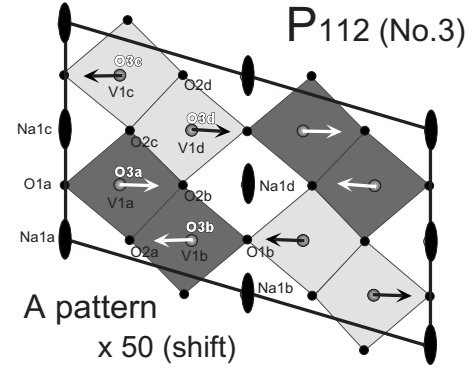


FIG. 4. The structural model of C_0 phase based on the space group C_2^1-P112 (No. 3). This structure is pulled out from one layer of $C_{1/4}$ phase, A pattern in Fig. 2. Black pyramids represent V^{4+}O_5 and white pyramids represent V^{5+}O_5 . Determined shifts of the vanadium ions, which are 50 times longer than the determined ones, are selectively shown by arrows.

Based on the structure parameters shown in Table I, we obtained the structure factor F of the C_0 phase. Then we calculated the intensity by taking the domain structures, the A and B patterns grown in the C_0 phase, into account as follows:

$$|I|_{\text{cal}} = \sum_{i=A,B} a_i |F_i|^2 L, \quad (4)$$

where F_A and F_B are the structure factors of the A and B patterns (see Fig. 2), and L is the Lorentz factor. a_A and a_B are the existence ratios of each domain. The ratio is defined as $a_A : a_B = \gamma : (1 - \gamma)$, where γ is one of the parameters for the present calculation. The final optimized parameter values are $\alpha=0.274$, $\beta=0.63$, and $\gamma=0.43$.

Figure 5 displays the observed (black circles) and calculated intensities (vertical solid lines). The calculated intensities reproduce the observed intensity oscillations well. It is especially important that there is no serious superlattice Bragg spot which is observable, but is not reproduced by the proposed model. We also show the plot of observed intensities $|I|_{\text{obs}}$ versus calculated intensities $|I|_{\text{cal}}$ in Fig. 6. All points follow the line of $|I|_{\text{cal}} = |I|_{\text{obs}}$, which shows that the present model calculation goes well and the extinction effect is negligible in the present study. Finally, we calculated that the discrepancy factor [R factor: $R(I) = \sum |I|_{\text{obs}} - |I|_{\text{cal}} / \sum |I|_{\text{obs}}$] for fundamental Bragg intensity was $R_F(I) = 12.7\%$ and that for superlattice Bragg intensity was $R_S(I) = 20.0\%$. Since the temperature dependence of the superlattice intensity already saturates at 6 K,²⁶ the factor $\alpha=0.274$ indicates the reduction ratio of the atomic shifts by the pressure application $P = 1.6 \text{ GPa}$. Incidentally, the factor $\beta=0.63$ also shows the reduction ratio of the amplitude of the atomic vibrations.

Note that since it is impossible to separate the domains experimentally at the C_0 phase, the observed form factor of each domain is not determined. We, therefore, adopted not $R(F)$ but $R(I)$ as the discrepancy factor. Then the value of $R(I)$ is overestimated rather than that of $R(F)$. In the case of the fundamental Bragg reflections, we can derive F_o and

TABLE I. Structure parameters used in the model calculation are shown. Basic crystallographic sites and initial atomic coordinates of each atom are used for structure determination of the C_0 phase. $(x, y, z)_{100\text{ K}}^{0.1\text{ MPa}}$ are the atomic coordinates at 100 K and ambient pressure (above T_C , P_{mmn}) (Ref. 17) adapted to $P112$ setting. $(\Delta x, \Delta y, \Delta z)_{10\text{ K}}^{0.1\text{ MPa}}$ is the atomic shift from $(x, y, z)_{100\text{ K}}^{0.1\text{ MPa}}$ derived from the A pattern of the $C_{1/4}$ phase. (Ref. 17) Shifts of vanadium ions can be visually seen in Fig. 4.

Atom	Site	x ,	y ,	$z)_{100\text{ K}}^{0.1\text{ MPa}}$	$(\Delta x$,	Δy ,	$\Delta z)_{10\text{ K}}^{0.1\text{ MPa}}$	$B_{10\text{ K}}^{0.1\text{ MPa}}$
Na1a	a	0	0	0.8572	0	0	-0.0024	0.36
Na1b	b	0.5	0	0.1428	0	0	-0.002	0.46
Na1c	c	0	0.5	0.8572	0	0	0	0.45
Na1d	d	0.5	0.5	0.1428	0	0	-0.0024	0.49
V1a	e	0.15219	0.326095	0.39046	0.00159	0.000595	-0.00394	0.18
V1b	e	0.34781	0.173905	0.60954	-0.00249	-0.001195	0.00834	0.21
V1c	e	0.15219	0.826095	0.39046	-0.00141	-0.000905	0.00486	0.21
V1d	e	0.34781	0.673905	0.60954	0.00241	0.000905	-0.00726	0.20
O1a	e	0	0.25	0.5187	-0.002	0.0012	-0.0069	0.38
O1b	e	0.5	0.25	0.4813	0.0012	-0.001	-0.0091	0.24
O2a	e	0.17704	0.08852	0.5117	-0.00106	-0.00248	0.0025	0.26
O2b	e	0.32296	0.41148	0.4883	-0.00024	0.00148	-0.0025	0.49
O2c	e	0.17704	0.58852	0.5117	0.00084	0.00052	-0.0011	0.27
O2d	e	0.32296	0.91148	0.4883	-0.00214	-0.00252	0.0047	0.41
O3a	e	0.13515	0.317575	0.0521	0.00085	0.002575	-0.0043	0.49
O3b	e	0.36485	0.182425	0.9479	0.00205	-0.001575	0.0067	0.32
O3c	e	0.13515	0.817575	0.0521	0.00155	0.005575	0.0041	0.49
O3d	e	0.36485	0.682425	0.9479	0.00155	-0.003575	-0.0061	0.31

$R_F(F)=8.0\%$, because those are unrelated to the domain formation. This factor is smaller than $R_F(I)=12.7\%$. This shows that the discrepancy factor using intensity gives worse values than those using the observed form factor.

Generally, the valence of an ion site under ambient pressure is empirically estimated using the information on atomic parameters such as bond length and coordination number. In the case of NaV_2O_5 , the valence of all vanadium ion sites at 10 K and ambient pressure ($C_{1/4}$ phase) was estimated as seen in Refs. 16 and 17. Our present results show that the atomic shift decreases down to 27% under 1.6 GPa at 6 K. We wondered whether the valence at each vanadium ion site decreases proportionally after the atomic shift reduces. To clarify the relation of the charge and the lattice under HP, we have investigated with RXS at LTHP around the V K -absorption edge (5.465 keV). RXS probes the charge modulation well.^{12,14,15} Experiments were performed on a four circle diffractometer installed at BL-16A2 (PF).

IV. CHARGE DISPROPORTIONATION IN THE C_0 PHASE

We have focused on a series of the energy scans at $15/2$ $1/2$ L ($L=1/4$ and 0). These superlattice spots are indexed by using the orthorhombic unit cell of RT phase. It is well confirmed that the energy profile of $15/2$ $1/2$ L peak at ambient pressure is realized by the dominant contribution from the charge ordering with $2a \times 2b \times 4c$ super structure.^{12,14,15}

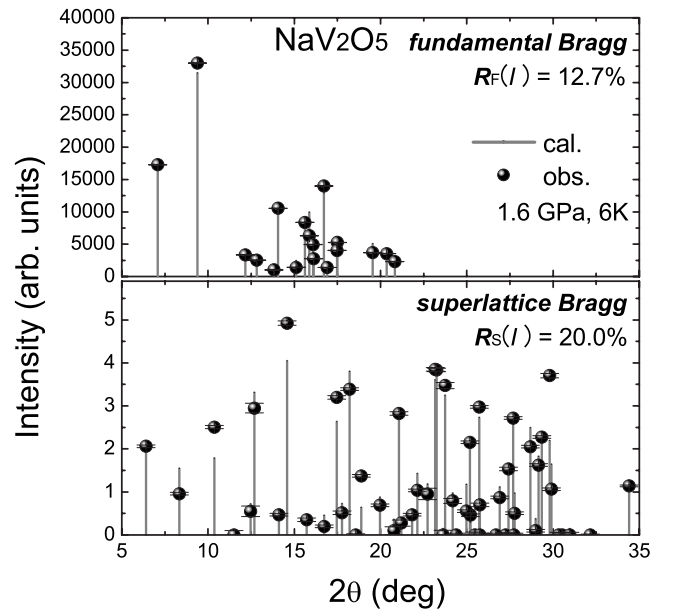


FIG. 5. Observed fundamental Bragg intensities vs calculated intensities (upper panel). Observed superlattice Bragg intensities vs calculated intensities (lower panel). We obtained the discrepancy factors for fundamental Bragg intensities as $R_F(I)=12.7\%$ and for superlattice Bragg intensities as $R_S(I)=20.0\%$. The adjustable parameters α , β , and γ are obtained as 0.274, 0.63, and 0.43, respectively.

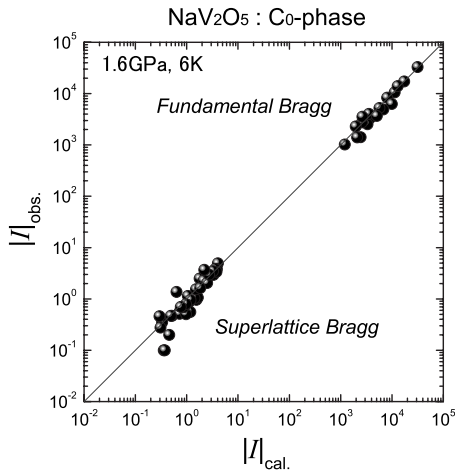


FIG. 6. Plot of $|I|_{\text{cal}}$ versus $|I|_{\text{obs}}$ taking into account the optimized scaling factors $\alpha=0.274$, $\beta=0.63$, and $\gamma=0.43$. The observed intensities $|I|_{\text{obs}}$ are well described by the present model.

The calculated off-resonant intensities at $L=1/4$ and 0 are approximately equal when we posit the same amount of atomic shift at the $C_{1/4}$ and C_0 phases. Also, the energy profile at $15/2\ 1/2\ 0$ can be reproduced by making the contribution from the charge order with $2a \times 2b \times 1c$ unit cell dominant. Thus, the intensities at $L=0$ and $L=1/4$ are directly comparable with each other without a scaling factor. The observed energy spectra at each pressure are displayed in Fig. 7(a), where $L=1/4$ ($C_{1/4}$ phase) at 0.1 MPa, $1/4$ ($C_{1/4}$ phase) at 0.6 GPa, and 0 (C_0 phase) at 1.2 GPa, respectively. For understanding the pressure dependence of the spectra, we divide it into three regions as follows: (i) E_A (pre-edge) the region around 5.468 keV with a single and sharp peak structure, (ii) E_B (main edge) the region around 5.475 keV with a double peak structure, and (iii) E_C the region above 5.480 keV with a multiple peak structure. The regions exhibit different pressure dependence patterns. As pressure increases, the peaks at E_A and E_C show a large reduction, while the peaks at E_B are almost constant.

In the case of NaV_2O_5 , the resonant spectrum caused by the charge order is largely determined by the difference in the anomalous dispersion of the ions V^{4+} and V^{5+} . The difference in the K -absorption energy of the two creates a large resonant intensity at the absorption edge. When the charge order develops, only the amplitude of the spectrum changes, but the spectrum shape is similar. That can be seen in the temperature dependence of the spectrum.^{15,23} However, the present spectrum exhibits no similar change of the spectrum shape as a result of the pressure application. This means that the changes do not simply reflect the increase and decrease of the degree of the charge order.

In order to confirm such crucial properties, we have also studied the pressure dependence of the fluorescence spectrum of NaV_2O_5 . Figure 7(b) shows the fluorescence spectra taken at $P=0.1$ MPa, 1.4 GPa, and 1.7 GPa at RT. Data were taken at BL22XU of SPring-8.²⁵ The intensities decrease as the pressure increases in the energy regions corresponding to E_A and E_C , while the intensity is constant at the energy region corresponding to E_B . As is well known, fluorescence

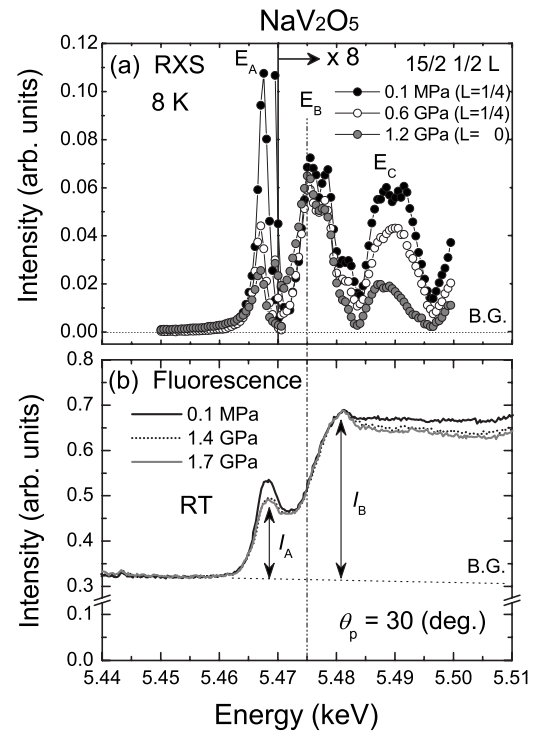


FIG. 7. (a) The energy scans at $Q=(15/2\ 1/2\ L)$ observed at 0.1 MPa ($L=1/4$, $C_{1/4}$ phase), 0.6 GPa ($L=1/4$, $C_{1/4}$ phase), and 1.2 GPa ($L=0$, C_0 phase) at 8 K. Note that the intensities above 5.47 keV are multiplied by 8. (b) Pressure dependence of the fluorescence spectra from NaV_2O_5 taken at 0.0, 1.4, and 1.7 GPa. Note that $\theta_p=30^\circ$.

intensity yields essentially the same results as more conventional *transmission* experiments.²⁸ That is, the present change of the fluorescence spectrum corresponds to the change of the x-ray anomalous dispersion of vanadium ions.

First, we discuss the resonant peaks at E_B of Fig. 7(a). The intensities at E_B are dominated by the difference in the main-edge energy of the V^{4+} and V^{5+} ions, which is a result of the charge disproportionation. The intensities at E_B show directly the degree of the charge disproportionation. From the pressure dependence pattern in Fig. 7(a), we can conclude that the intensities at E_B are not dependent on the structural change caused by pressure, in other words, charges in all vanadium sites become disproportionate, even though atomic shifts are suppressed by an increase in the pressure application. We could not reach 1.6 GPa in this work because of the limited strength of the Be gasket, but our conclusion that there is full charge disproportionation in spite of the reduction of the atomic shifts under HP is unchanged. Because of this full charge disproportionation, the intensities at E_A and E_C should not change if the amplitude and shape of the anomalous dispersion are not changed by the pressure. However, the present results show large intensity reduction at E_A and E_C under increased pressure. There should be some other factors causing this.

Secondly, the reduction of the resonant intensity at E_A of Fig. 7(a) will be discussed. We calculated the ratio I_A/I_B as shown in Fig. 8(a), where the intensities I_A and I_B are defined as shown in Fig. 7(b). This ratio clearly decreases as the

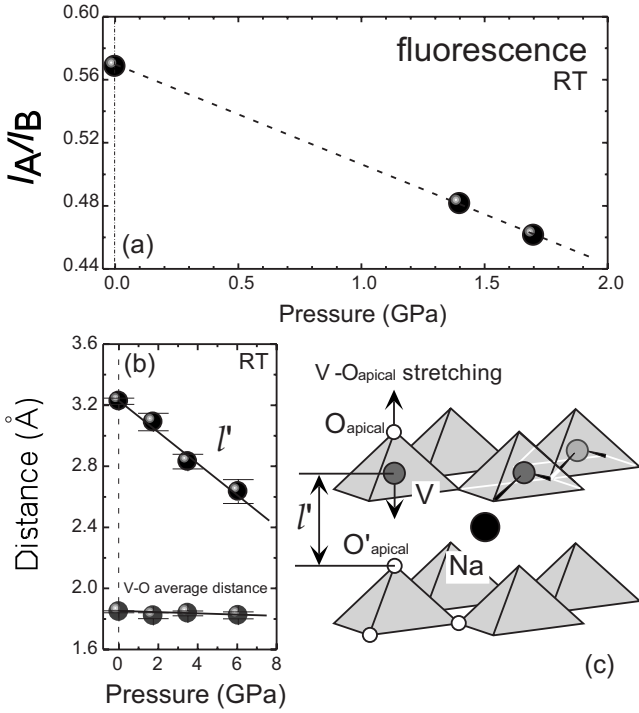


FIG. 8. (a) Pressure dependence of I_A/I_B at RT derived from Fig. 7(b). (b) Pressure dependence of the V—O'_{apical} distance l' at RT (Ref. 27) (c) The V—O'_{apical} distance and l' are defined as shown.

pressure increases. We can understand qualitatively that the intensity reduction seen at E_A is due to the reduction of amplitude of anomalous dispersion f' and f'' at the pre-edge. A first principles calculation²⁴ predicts this reduction of the pre-edge amplitude of the absorption spectrum of V_2O_5 . It arises from deactivation of the $1s \rightarrow 3d$ dipole transition due to the reduction of antisymmetry around V ion ($O=V \cdots O$) along the c axis. Such a reduction of the antisymmetry is already realized by pressure application as shown in Figs. 8(b) and 8(c).²⁷ The V—O'_{apical} distance (l') of NaV_2O_5 is known to be strongly compressible, while the V—O_{apical} distance is only slightly affected by the pressure application.^{27,29} Therefore, the $O_{apical}=V \cdots O'_{apical}$ antisymmetry along the c axis can be improved by the pressure application.

The reduction of the RXS amplitude at E_C of Fig. 7(a) may be related to the reduction of the amplitude of the fluorescence, however, we do not have a clear explanation for this at present. If we can obtain the pressure dependence of the anomalous dispersion of V^{4+} and V^{5+} ions, the nature of the change at E_C will be clarified.

Finally, the results of the RXS and fluorescence measurements led to two important conclusions. (i) The charges become fully disproportionate under high pressure. (ii) The amplitude of the anomalous dispersion of the vanadium ions at E_A and E_C regions is also greatly changed.

Incidentally, this is a case where a first principles calculation²⁴ concerning the pre-edge amplitude of vanadium ion has been confirmed by a pressure experiment.

V. DISCUSSION

A. Ising spin-phonon coupling

Let us first discuss the Ising variable in NaV_2O_5 . As demonstrated in Secs. II and III, charges become fully disproportionate in spite of the large suppression of the atomic shifts by the pressure application. The small reduction of the spin-gap energy measured by neutron scattering was at most -1 meV/GPa,³⁰ which supports our findings that the charges become fully disproportionate under HP. By taking these facts into account, we postulate that charge disproportionation is the Ising variable (=the primary order parameter) in NaV_2O_5 . Atomic shifts, which are observable by a conventional nonresonant x-ray diffraction, are also regarded as linearly coupled to this variables.

Then, we can deduce that NaV_2O_5 can be characterized by a strong linear coupling of the Ising system (charge disproportionation) to a phonon mode (atomic shifts), as can be seen in the typical Ising systems NH_4Br (Ref. 31) and A_2BX_4 ($A=K, Rb$, and NH_4 ; $X=Cl$ and Br).³² In such a linear coupled system, the temperature dependence of the primary order parameter and that of the coupled atomic shift exhibit the same behavior. In the case of NaV_2O_5 , the behavior of each component is similar, which is shown by the temperature dependence of the intensities of the superlattice reflection both at energies reflecting the charge ordering (on-resonant) and at those reflecting atomic shifts (off-resonant).¹²

By the canonical transformation of the phonon coordinates, the Hamiltonian of the spin-phonon linearly coupled system can be expressed as a simple pair interaction Hamiltonian, where an effective pair interaction J_{eff} is introduced.³¹ Including the spin-phonon coupling term, the total microscopic Hamiltonian for the spin-phonon coupled system is generally set as follows:

$$H = \frac{1}{2} \sum_{\mathbf{k},s} (p_{\mathbf{k},s} p_{\mathbf{k},s}^* + \omega_{\mathbf{k},s}^2 q_{\mathbf{k},s} q_{\mathbf{k},s}^*) - \frac{1}{2} \sum_{ij} J_{ij} \sigma_i \sigma_j - \sum_{\mathbf{k},s} \sum_i \frac{\omega_{\mathbf{k},s}}{\sqrt{N}} g_{\mathbf{k},s} q_{\mathbf{k},s} \sigma_i e^{ikr_i}, \quad (5)$$

where $q_{\mathbf{k},s}$ is the phonon coordinate with wave number \mathbf{k} and mode s , $\omega_{\mathbf{k},s}$ is the characteristic frequency of the corresponding phonon, N is the number of the unit cells in the system, $p_{\mathbf{k},s}$ is a canonical conjugate of $q_{\mathbf{k},s}$, J_{ij} is the pair interaction energy between σ_i and σ_j separated by the vector r_{ij} , and $g_{\mathbf{k},s}$ is a spin-phonon coupling constant. Following the canonical transformation given in Ref. 31, the Hamiltonian is expressed in a normalized form as:

$$H_{\text{eff}} = \frac{1}{2} \sum_{\mathbf{k},s} (P_{\mathbf{k},s} P_{\mathbf{k},s}^* + \omega_{\mathbf{k},s}^2 Q_{\mathbf{k},s} Q_{\mathbf{k},s}^*) - \frac{1}{2} \sum_{ij} J_{\text{eff}} \sigma_i \sigma_j, \quad (6)$$

where the effective pair interaction energy J_{eff} between spins is given by

$$J_{\text{eff}} = \sum_{\mathbf{k},s} \frac{1}{N} g_{\mathbf{k},s} g_{\mathbf{k},s}^* e^{ik(r_i - r_j)} + J_{ij}. \quad (7)$$

Since the entire interaction is reduced to the J_{eff} , which contains the Ising spin-phonon coupling constants $g_{k,s}$, the Ising spin-phonon-coupled ANNNI model can be handled as the usual ANNNI model. The important requirement of such an Ising spin-phonon-coupled system is that the interaction between the Ising spins can be mediated by a phonon mode over a long range. Such a long range interaction is introduced to describe the devil's flower in A_2BX_4 type dielectric materials,³² where the third nearest neighbor interaction is considered. This feature also makes it possible to introduce pressure sensitivity to the interaction ratio $-J_2/J_1$ in the ANNNI system as observed in NaV_2O_5 . It will be difficult to explain a change in the positive and/or negative sign of the interaction to $J_1 \geq 0$, $J_2 \leq 0$, or a drastic change in the interaction ratio $-J_2/J_1$ by the repulsive Coulomb interaction only.

Since the Ising spins are constructed by the arrangement of the charges, the attractive interaction J_1 is difficult to derive from Coulomb repulsion alone. The present discussion of the *Ising spin-phonon coupling* holds the key to generating the attractive interaction J_1 between Ising spins. Such an attractive interaction between the Ising spins is seen in ferroelectric LuFe_2O_4 , where \uparrow when the unit cell is occupied by the Fe^{2+} ions and \downarrow when the unit cell is occupied by the Fe^{3+} ions.³³ In this case, the authors view the origin of the attractive interaction from a macroscopic view point, hypothesizing that a charge on the Fe site will induce polarization in the surrounding dielectric medium which overscreens the core charge at some distance. The charge placed at a distance feels the attractive interaction. From a microscopic viewpoint, the authors suggest that the excess charge on the Fe site tends to induce displacement of the surrounding oxygen ions so that small polarons are formed.³³

In the case of NaV_2O_5 , large pressure effects on some phonon modes were found by Raman scattering at room temperature by Loa *et al.*^{34,35} Raman scattering accurately reveals the phonon frequency at momentum transfer $\Delta Q=0$. For example, the electron-phonon coupled mode at 453 cm^{-1} (Ref. 34) is found to be particularly sensitive to pressure, with a rate of $6 \text{ cm}^{-1}/\text{GPa}$, while the $\text{V}=\text{O}_{\text{apical}}$ out-of-plane stretching mode at 972 cm^{-1} exhibits major softening, $-4 \text{ cm}^{-1}/\text{GPa}$. The above results clearly reveal that there are some phonon modes which are very sensitive to the pressure. However, we do not know which mode couples to the charge disproportionation and provides the competing interactions $J_2 \leq 0$ and $J_1 \geq 0$ at present. Precise study of the phonon dispersions will be needed as seen in the neutron scattering investigation of K_2SeO_4 .³⁶

B. Complex behavior near T_C

Finally, we will discuss the remaining question of behavior under ambient pressure ($C_{1/4}$ phase), particularly the complex behavior experimentally observed near T_C . Köppen *et al.* found out two adjacent phase transitions by thermal expansion measurement: $T_1=33.0 \pm 0.1 \text{ K}$ and $T_2=32.7 \pm 0.1 \text{ K}$.³⁷ Moreover, by the ^{51}V NMR and ^{23}Na NMR measurements, Ohama *et al.* found coexisting resonance lines of the uniform and charge-ordered phases between 33.4

and 33.8 K.^{9,38} They have a temperature width similar to the ones observed in the thermal expansion measurements. Since NaV_2O_5 is supposed to be an ideal ANNNI system, we propose that it is possible to describe the phenomenon which happens in the temperature range $\Delta T \sim 0.4 \text{ K}$ with this system.

Figure 9 shows the characteristic properties of (a) T_C , (b) q_c at T_C , and (c) q_c at 0 K of the ANNNI system.³⁴ One can see from Figs. 9(a)–9(c) that the phase with $q_c=1/4$ never appears just below T_C without going by way of an incommensurate phase with $q_c \neq 0$ when $-J_2/J_1 < 1/4$ (=Lifshitz point). Namely, $-J_2/J_1 \rightarrow \infty$ ($J_1 \rightarrow 0$ or $J_2 \rightarrow -\infty$) is needed for the appearance of the phase with $q_c=1/4$ just at T_C . When we consider that the $-J_2/J_1$ of NaV_2O_5 has a finite value at ambient pressure, NaV_2O_5 will exhibit the incommensurate phase just below T_C within the narrow temperature range $\Delta T \sim 0.4 \text{ K}$ at ambient pressure, as observed in thermal expansion and NMR measurements. It is difficult to observe such an incommensurate momentum transfer by the present x-ray measurement because of the weak intensity and small momentum transfer from $q_c=1/4$ just below T_C at ambient pressure, and it will be a challenging task for us to find such an incommensurate phase.

We also show the pressure scale of NaV_2O_5 in Fig. 9. It is very surprising that the ratio of $-J_2/J_1$ in NaV_2O_5 can be changed by as much as a factor of $10-10^2$ by the application of only about 1 GPa pressure. As discussed above, large effects of pressure on some phonon modes, and major softening of the $\text{V}=\text{O}_{\text{apical}}$ out-of-plane stretching mode at 972 cm^{-1} and the electron-phonon coupled mode at 453 cm^{-1} ,³⁴ may play a part in the large change in the interaction ratio of $-J_2/J_1$ in NaV_2O_5 .

VI. SUMMARY

We have studied the ground state of NaV_2O_5 under HP, which is the so-called C_0 phase. It has been shown that the structure of such a C_0 phase can be explained by one layer, the A pattern in Fig. 2 which is taken from the AAA'A' sequence of the $C_{1/4}$ phase, on condition that the amount of atomic shifts decreases under HP. The space group of C_0 phase was determined to be $P112$ monoclinic, which is a subgroup of $A112$, the space group of $C_{1/4}$ phase. From the analysis of model calculation based on $P112$, the amount of the atomic shifts at 1.6 GPa and 6 K is found to decrease down to 27% under ambient pressure. To study the valence states at each ion under HP, we measured a series of RXS spectra under 0.1 MPa, 0.6 GPa, and 1.2 GPa at 6 K. The intensity does not change with pressure at 5.475 keV, where it is mainly dominated by the edge-energy difference between V^{4+} and V^{5+} , indicating clearly that there is full charge ordering in spite of the suppression of atomic shifts by the pressure application. Based on these facts, charge disproportionation is regarded as an order parameter and Ising variable in NaV_2O_5 . Atomic shifts are regarded as linearly coupled to the Ising spins.

The existence of the Ising spin (charge arrangement)-phonon coupling in NaV_2O_5 has been demonstrated in the present study. However, the detailed investigation of micro-

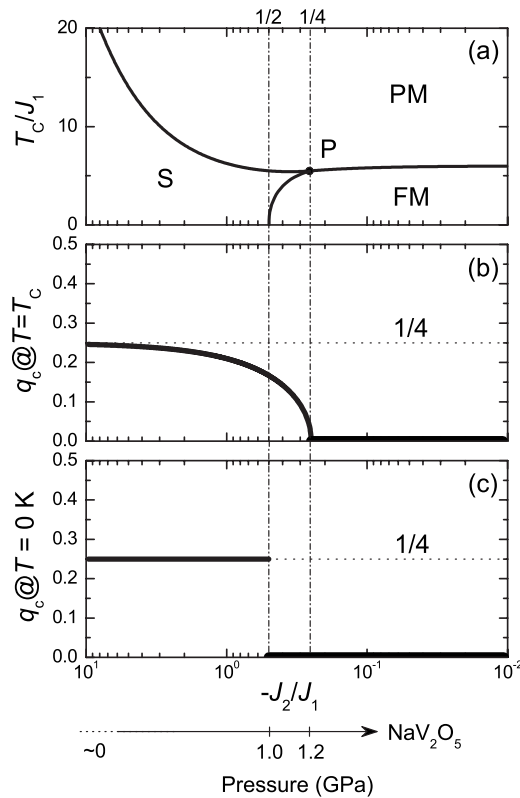


FIG. 9. Characteristic properties of T_C and q_c of the ANNNI system. (a) T_C as a function of $-J_2/J_1$. PM, paramagnetic; FM, ferromagnetic; S, sinusoidal; P, Lifshitz point. [(b) and (c)] q_c at T_C and 0 K as a function of $-J_2/J_1$, respectively. We can see only two ground states with $1/4$ and 0 . The pressure scale in the case of NaV_2O_5 system is also shown.

scopic mechanisms on the interactions J_1 and J_2 remains an important subject to be solved in the near future.

Finally, we would like to mention some interesting predictions of the ANNNI system. One is the ANNNI model *in external fields*,³⁹ and the other is *diluted ANNNI model*.⁴⁰ In the former case, the devil's flower under the external field is expected to change drastically. However, an external field affecting the Ising spin (charge ordering) in NaV_2O_5 has not been found as yet. High magnetic field^{41–43} is not the external field for the present ANNNI system. In the latter case, the Na deficiency can control the Ising spin density in the NaV_2O_5 system. The effect of the dilution of the spin density to the ANNNI system should be interesting.

ACKNOWLEDGMENTS

We would like to thank E. Ninomiya (TDK Corporation), H. Sawa (KEK-PF), M. Nishi (ISSP, The University of Tokyo), and H. Seo (JAEA) for stimulating discussions, as well as K. Ishii (JAEA) for technical support. K.O. gives special thanks to T. Mori. This work was supported in part by a Grant-In-Aid for Scientific Research from MEXT (Proposal No. 14740221) and by the RIKEN NOP project under the support from the Special Coordination Funds for Promoting MEXT. The x-ray experiments were performed at the SPring-8 with the approval of the Japan Synchrotron Radiation Research Institute (JASRI) (Proposal No. 2002B0277-ND1-np and No. 2003A2277-CD1-np), and at the Photon Factory with the approval of the Advisory Committee (Proposal No. 2001G255). RXS-DAC was developed in collaboration with the late N. Toyoshima.

*Also at CREST, Japan Science and Technology Agency; ohwada@spring8.or.jp

†Present address: All Nippon Airways Co., Ltd., Japan.

‡Present address: Okayama University, 1-1-1 Tsushima, Okayama, Okayama 700-8530, Japan.

¹K. Ohwada *et al.*, Phys. Rev. Lett. **87**, 086402 (2001).

²K. Ohwada, H. Nakao, H. Nakatogawa, N. Takesue, Y. Fujii, M. Isobe, Y. Ueda, Y. Wakabayashi, and Y. Murakami, J. Phys. Soc. Jpn. **69**, 639 (2000).

³P. Bak and J. von Boehm, Phys. Rev. B **21**, 5297 (1980).

⁴P. Bak, Rep. Prog. Phys. **45**, 587 (1982).

⁵M. Isobe and Y. Ueda, J. Phys. Soc. Jpn. **65**, 1178 (1996).

⁶H. Smolinski, C. Gros, W. Weber, U. Peuchert, G. Roth, M. Weiden, and C. Geibel, Phys. Rev. Lett. **80**, 5164 (1998).

⁷H. Seo and H. Fukuyama, J. Phys. Soc. Jpn. **67**, 2602 (1998).

⁸K. Tsuda, S. Amamiya, M. Tanaka, Y. Noda, M. Isobe, and Y. Ueda, J. Phys. Soc. Jpn. **69**, 1939 (2000).

⁹T. Ohama, H. Yasuoka, M. Isobe, and Y. Ueda, Phys. Rev. B **59**, 3299 (1999).

¹⁰Y. Fujii, H. Nakao, T. Yosihama, M. Nishi, K. Nakajima, K. Kakurai, M. Isobe, Y. Ueda, and H. Sawa, J. Phys. Soc. Jpn. **66**, 326 (1997).

¹¹T. Yosihama, M. Nishi, K. Nakajima, K. Kakurai, Y. Fujii, M. Isobe, C. Kagami, and Y. Ueda, J. Phys. Soc. Jpn. **67**, 744 (1998).

¹²H. Nakao *et al.*, Phys. Rev. Lett. **85**, 4349 (2000).

¹³Y. Fujii *et al.*, Solid State Phys. (Tokyo) **37**, 627 (2002).

¹⁴K. Ohwada, Y. Fujii, Y. Katsuki, J. Muraoka, H. Nakao, Y. Murakami, H. Sawa, E. Ninomiya, M. Isobe, and Y. Ueda, Phys. Rev. Lett. **94**, 106401 (2005).

¹⁵K. Ohwada, Y. Fujii, H. Nakao, Y. Murakami, M. Isobe, and Y. Ueda, Mod. Phys. Lett. B **20**, 199 (2006).

¹⁶H. Sawa, E. Ninomiya, T. Ohama, H. Nakao, K. Ohwada, Y. Murakami, Y. Fujii, Y. Noda, M. Isobe, and Y. Ueda, J. Phys. Soc. Jpn. **71**, 385 (2002).

¹⁷E. Ninomiya, Ph.D. thesis, Chiba University, 2003.

¹⁸C. S. Menoni and I. L. Spain, High Temp. - High Press. **16**, 119 (1984).

¹⁹M. Isobe, C. Kagami, and Y. Ueda, J. Cryst. Growth **181**, 314 (1997).

²⁰H. K. Mao *et al.*, Science **292**, 914 (2001).

²¹J. Garcia and M. Benfatto, Phys. Rev. Lett. **87**, 189701 (2001).

²²J. E. Lorenzo, S. Bos, S. Grenier, H. Renevier, and S. Ravy, Phys. Rev. Lett. **87**, 189702 (2001).

- ²³H. Nakao *et al.*, Phys. Rev. Lett. **87**, 189703 (2001).
- ²⁴O. Šipr, A. Šimůnek, S. Bocharov, T. Kirchner, and G. Dräger, Phys. Rev. B **60**, 14115 (1999).
- ²⁵T. Shobu, K. Tozawa, H. Shiwaku, H. Konishi, T. Inami, T. Harami, and J. Mizuki, AIP Conf. Proc. No. 879 (AIP, New York, 2007), p. 902.
- ²⁶K. Ohwada, Ph.D. thesis, The University of Tokyo, 2001.
- ²⁷K. Ohwada, H. Nakao, Y. Fujii, M. Isobe, and Y. Ueda, J. Phys. Soc. Jpn. **68**, 3286 (1999).
- ²⁸J. Jaklevic, J. A. Kirby, M. P. Klein, A. S. Robertson, G. S. Brown, and P. Eisenberger, Solid State Commun. **23**, 679 (1977).
- ²⁹I. Loa, K. Syassen, R. K. Kremer, U. Schwarz, and M. Hanfland, Phys. Rev. B **60**, R6945 (1999).
- ³⁰M. Nishi *et al.*, Neutron Scattering Research, ISSP University of Tokyo Report No. 9, 2002, p. 156.
- ³¹Y. Yamada, M. Mori, and Y. Noda, J. Phys. Soc. Jpn. **32**, 1565 (1972).
- ³²Y. Yamada and N. Hamaya, J. Phys. Soc. Jpn. **52**, 3466 (1983).
- ³³Y. Yamada, K. Kitsuda, S. Nohdo, and N. Ikeda, Phys. Rev. B **62**, 12167 (2000).
- ³⁴I. Loa, K. Syassen, and P. K. Kremer, Solid State Commun. **112**, 681 (1999).
- ³⁵I. Loa, U. Schwarz, M. Hanfland, P. K. Kremer, and K. Syassen, Phys. Status Solidi B **215**, 709 (1999).
- ³⁶M. Iizumi, J. D. Axe, G. Shirane, and K. Shimaoka, Phys. Rev. B **15**, 4392 (1977).
- ³⁷M. Köppen, D. Pankert, R. Hauptmann, M. Lang, M. Weiden, C. Geibel, and F. Steglich, Phys. Rev. B **57**, 8466 (1998).
- ³⁸T. Ohama, A. Goto, T. Shimizu, E. Ninomiya, H. Sawa, M. Isobe, and Y. Ueda, J. Phys. Soc. Jpn. **69**, 2751 (2000).
- ³⁹J. Randa, Phys. Rev. B **32**, 413 (1985).
- ⁴⁰T. Kawasaki, Prog. Theor. Phys. **71**, 246 (1984).
- ⁴¹W. Schnelle, Y. Grin, and R. K. Kremer, Phys. Rev. B **59**, 73 (1999).
- ⁴²S. G. Bompadre, A. F. Hebard, V. N. Kotov, D. Hall, G. Maris, J. Baas, and T. T. M. Palstra, Phys. Rev. B **61**, R13321 (2000).
- ⁴³A. B. Sushkov, J. L. Musfeldt, S. A. Crooker, J. Jegoudez, and A. Revcolevschi, Phys. Rev. B **63**, 220401(R) (2001).